High-Spatial-Resolution and Wide-Range Strain Distributed Sensor Based on Exposed-SMF Using Efficient Adaptive Zero Padding

Cailing Fu, Chao Du, Rongyi Shan, Zhenwei Peng, Ronglong Sui, Huajian Zhong, Yanjie Meng, Wenfa Liang, Shuai Xiao, Yuhao Kong, Xiaoyu Yin, and Yiping Wang, *Senior Member, IEEE*

***Abstract*—A high-spatial resolution and wide-range distributed strain sensor (DSS) based on UV laser exposed single mode fiber (E-SMF) has been experimentally demonstrated, of which the maximum measurable strain was up to 9000 $\mu\varepsilon$ under a spatial resolution of 1.5 mm. To address the tradeoff between strain resolution and sensing spatial resolution, an efficient adaptive zero padding (AZP) was proposed to calculate the number of padding zeros to optimize the number of zero padding (NZP). Compared with traditional zero padding (TZP), the cross correlation calculation time was improved from 138.842 to 0.476 s using the proposed AZP method under the spatial resolution of 1.5 mm, indicating that the cross correlation calculation time was reduced by nearly 300×. Moreover, the distance compensation method (DCM) was employed to improve the deteriorated similarity induced by position deviation between the reference (Ref.) and measurement (Mea.) signal, which could be greatly improved by using DCM. The strain property of the E-SMF and SMF was compared and investigated by DCM based on the AZP method. The strain profile of the E-SMF could be successfully and well demodulated in the zero- and stretched-strain section at the spatial resolution of 1.5 mm by using DCM, when the applied strain was increased from 1000 to 9000 $\mu\varepsilon$.**

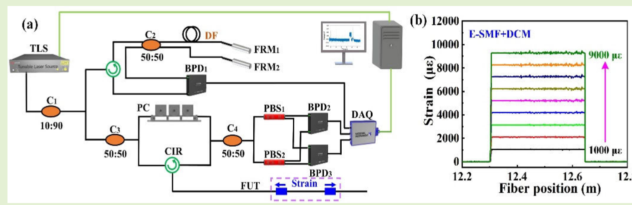

***Index Terms*— Distance compensation method (DCM), distributer strain sensor (DSS), exposed single mode fiber (E-SMF), optical frequency domain reflectometry.**

I. Introduction

OPTICAL fiber sensor has attracted intensive applications in civil, structural, health [1], pipeline security [2], life and health monitoring [3], [4], [5], [6], [7]. Among them, distributed fiber sensor has attracted great attention [8]. Especially, various distributed strain sensor (DSS) with high spatial resolution and wide measurement (Mea.) range have been proposed and demonstrated. Compared with optical time-domain reflectometry [9], DSS using the same scattering, i.e., Rayleigh backscattering (RBS), based on optical frequency domain reflectometer (OFDR) could achieve a sub-centimeter spatial resolution [10]. However, the weak RBS (−100 dB/mm) of the OFDR strain sensor is vulnerable to the nonlinear frequency modulation, cross correlation noise, and environmental disturbance of the tunable laser source (TLS), which degrades the similarity between the obtained reference (Ref.) spectrum and Mea. spectrum [11] and form fake peaks or multipeaks, further resulting in the misjudged spectrum shift [12]. In other words, the spatial resolution and Mea. range is limited by the weak RBS. To improve the signal-to-noise ratio (SNR) of the DSS, i.e., enhance the intrinsic RBS in single mode fiber (SMF), several post-processing methods, such as UV laser exposure [13], [14], femtosecond-laser-induced defects [15], [16], and random fiber gratings [17], were proposed. However, it is nonstandard, labor-intensive, and expensive to realize long-distance RBS enhancement by using laser micromachining technique [16]. In the meantime, various

Manuscript received 19 August 2023; revised 21 September 2023; accepted 21 September 2023. Date of publication 5 October 2023; date of current version 1 May 2024. This work was supported in part by the National Key Research and Development Program of China under Grant 2022YFE0111400; in part by the National Natural Science Foundation of China under Grant U22A2088 and Grant 62375178; in part by the Shenzhen Science and Technology Program under Grant JCYJ20200109114020865, Grant JCYJ20200109114201731, Grant JCYJ20200810121618001, and Grant JSGG20201102152200001; and in part by LingChuang Research Project of China National Nuclear Corporation under Grant CNNC-LCKY-202265. The associate editor coordinating the review of this article and approving it for publication was Prof. Santosh Kumar. *(Corresponding author: Yiping Wang.)*

The authors are with the Key Laboratory of Optoelectronic Devices and Systems of Ministry of Education/Guangdong Province, College of Physics and Optoelectronic Engineering, and the Shenzhen Key Laboratory of Photonic Devices and Sensing Systems for Internet of Things, Guangdong and Hong Kong Joint Research Center for Optical Fiber Sensors, Shenzhen University, Shenzhen 518060, China (e-mail: fucailing@szu.edu.cn; 2060453065@email.szu.edu.cn; 2200453068@email.szu.edu.cn; 1041562932@qq.com; 2100453058@email.szu.edu.cn; 2250453001@email.szu.edu.cn; mengyanjie2020@email.szu.edu.cn; 2210452035@email.szu.edu.cn; 2200453061@email.szu.edu.cn; 2210452110@email.szu.edu.cn; xyin@szu.edu.cn; ypwang@szu.edu.cn).

Digital Object Identifier 10.1109/JSEN.2023.3319479

1558-1748 © 2023 IEEE. Personal use is permitted, but republication/redistribution requires IEEE permission.
See https://www.ieee.org/publications/rights/index.html for more information.

Authorized licensed use limited to: SHENZHEN UNIVERSITY. Downloaded on October 29,2024 at 03:28:24 UTC from IEEE Xplore. Restrictions apply.

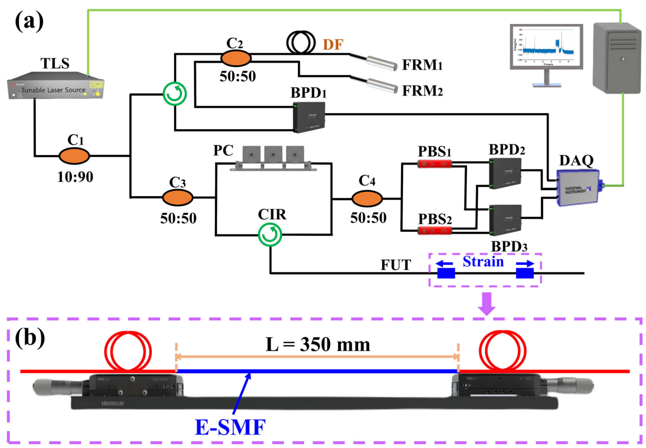

Fig. 1. (a) Experimental setup for distributed wide-strain sensing based on E-SMF. (b) Schematic of strain applied apparatus to E-SMF by using one linear translation stage. TLS: tunable laser source; C: coupler; PC: polarization controller; DF: delay fiber; FRM: faraday rotating mirror; BPD: balanced photo-detector; PBS: polarization beam splitter; CIR: circulator; and DAQ: data acquisition card.

algorithms have also been proposed [18], [19], [20], [21], [22]. For example, an image wavelet denoising method was proposed to suppress the noise, where the spatial resolution was 2.56 mm under strain of 2000 $\mu\varepsilon$ [18]. An approach based on local similarity of Rayleigh scattering (RS) spectrum method was also employed to eliminate fake and multi peaks, where the spatial resolution was 3.00 mm under strain of 3000 $\mu\varepsilon$ [19]. The position deviation caused by applied strain could be solved by distance compensation method (DCM), where the maximum measurable strain was 10 000 $\mu\varepsilon$ with a spatial resolution of 2.00 mm [20]. Although afore-mentioned algorithms could solve the spectral matching and spatial compensation, additional algorithms, such as local similarity and image wavelet denoising have brought a huge computational burden to the already complex OFDR data processing process. In addition, there is a tradeoff between the spatial resolution and Mea. range, that is, the spatial resolution has to be broadened for achieving wide strain Mea. range [20]. Therefore, a high-spatial-resolution and wide-range DSS without extra algorithm are in great demand.

In this article, a high-spatial-resolution and wide-range DSS based on exposed-SMF (E-SMF) using efficient adaptive zero padding (AZP) method was proposed and demonstrated. The influence of the number of zero padding (NZP) on the sensing spatial resolution and strain resolution was discussed to propose the AZP method. The deteriorated similarity due to large position deviation induced by large strain was also investigated. The strain property of the E-SMF and SMF was compared and investigated by DCM based on AZP. Furthermore, the performance of AZP and traditional zero padding (TZP) was compared.

II. Experimental Setup and Methods

The experimental setup based on a conventional OFDR system is illustrated in Fig. 1(a). The light from the TLS was split into two paths by a 10:90 optical coupler (C_1), where the scanning range and rate of the TLS were 1535–1565 nm and 100 nm/s, respectively. The 10% light was injected into an auxiliary Michelson interferometer, where two Faraday rotating mirrors (FRMs), i.e., FRM_1 and FRM_2, are implemented to reduce the polarization fading effect [23]. The generated signal was used as the external clock of the data acquisition card (DAQ) to sample the beat signal from a balanced photo-detector (BPD) at equidistant instantaneous optical frequency points. The 90% light was injected into the main Mach-Zehnder interferometer and split by a 50:50 optical coupler (C_3). Then, the RBS reflected by the fiber under test (FUT) was mixed with the Ref. light passing through the polarization controller (PC) by the C_4, where the PC was used to adjust the polarization state. A polarization diversity detection includes two polarization beam splitters (PBSs), i.e., PBS_1 and PBS_2, as well as two BPDs, i.e., BPD_2 and BPD_3, which are employed to reduce the polarization fading effects in the main interferometer. That is, two BPDs are used to separately acquire the divided p- and s-polarization light through two PBSs [23].

In the experiment, a UV laser E-SMF with an enhanced RBS intensity was employed as the strain sensor [14]. To achieve direct exposure, the coating of the SMF should be removed due to its opacity to the UV laser. As we know, any damage on the fiber surface will affect the maximum strain it can withstand. To achieve wide-range strain Mea., i.e., maintain the mechanical strength of the FUT, the fiber coating was removed by immersing it in acetone for 40 min instead of a fiber stripper. As shown in Fig. 1(b), two ends of the E-SMF were fixed on two 1-D linear translation stages via AB glue. The strain ranging from 0 to 9000 $\mu\varepsilon$ with a step of 1000 $\mu\varepsilon$ was applied by moving one linear translation stage along the fiber axis. Note that the initial distance between the two stages was 350 mm, i.e., $L = 350$ mm.

The traditional data processing based on OFDR is illustrated in Fig. 2(a). First, two beat signals in the optical frequency domain under different states, i.e., Ref. signal without strain and Mea. signal with strain were collected, respectively. Second, fast Fourier transform (FFT) was conducted to transform to the spatial domain along the entire FUT, i.e., obtaining an RBS profile as the distance function [16]. Third, the FUT was divided into multiple sections for the Ref. and Mea. signal, i.e., Ref(i) and Mea(i), by using a sliding window with a length of N, indicating that the number of sampling points in a sliding window was N. Generally, each sliding window was padded with (M–N) zeros to the initial number of total data, i.e., M, and transformed back to frequency domain through inverse FFT (IFFT). Finally, the cross correlation between Ref. and Mea. signal was performed to obtain the spectral shift, i.e., Δf. Then, the applied strain could be obtained according to the spectral shift between the Ref. and Mea. spectrum [21]. The two-point spatial resolution, i.e., Δz, in the distance domain could be given by the following equation:

$$\Delta z = c/2n\Delta F \tag{1}$$

where c is the light velocity in vacuum, n is the refractive index of the medium, and ΔF is the range of the sweep frequency of the TLS, i.e., $\Delta F = 3750$ GHz. Then, it could be calculated

Authorized licensed use limited to: SHENZHEN UNIVERSITY. Downloaded on October 29,2024 at 03:28:24 UTC from IEEE Xplore. Restrictions apply.

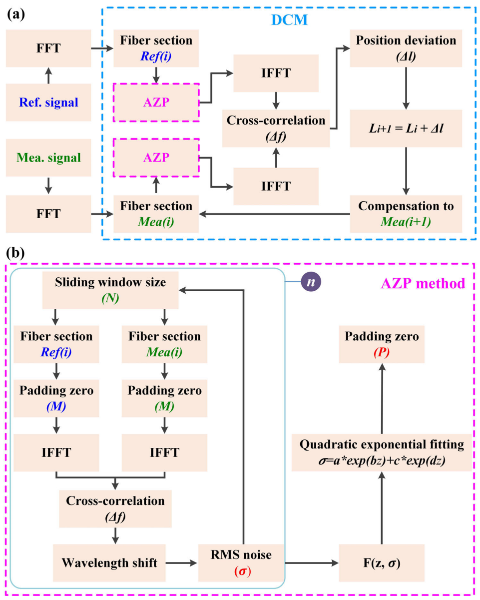

Fig. 2. (a) Flow diagram of the data processing based on OFDR using AZP and DC, and (b) detailed flow diagram of AZP method. Ref. signal: reference signal; Mea. signal: measurement signal; FFT: fast Fourier transformation; IFFT: inverse FFT; and Ref(i) and Mea(i) represents the ith reference and measurement signal in time-domain, respectively ($i = 1, 2, 3 \ldots$).

to 0.0275 nm, i.e., $\Delta z = 0.0275$ mm.In addition, the sensing spatial resolution, i.e., Z, could be given by the following equation:

$$Z = N\Delta z \tag{2}$$

where N is the number of data points and $N = 54$. Thus, the sensing spatial resolution is 1.5 mm, i.e., $Z = 1.5$ mm.

The strain resolution, i.e., $\Delta\varepsilon$, was proportional to the spectral shift between two cross correlation single points, i.e., Δf_{res}, which could be given by the following equation [18]:

$$\Delta f_{\mathrm{res}} = \Delta F/N. \tag{3}$$

In addition, the relationship between the sensing spatial, i.e., Z, and strain resolution, i.e., $\Delta\varepsilon$, could be given by the following equation [6]:

$$Z\Delta\varepsilon = \lambda/4n. \tag{4}$$

According to (1)–(4), the strain resolution, i.e., Δf_{res}, could be improved by using a longer sliding window, i.e., increasing the number of sampling point N, but the sensing spatial resolution, i.e., Z, would be deteriorated. The sampling rate could be increased by using the zero padding method to the signal before IFFT. When the sliding window was padded with (M–N) zeros to the initial number of total data, i.e., M, (3) would be changed into the following equation:

$$\Delta f_{\mathrm{res}} = \Delta F/(N + (M - N)) = \Delta FM. \tag{5}$$

In this way, the strain resolution, i.e., $\Delta\varepsilon$, could be restored by padding zero to the original data size, i.e., M, without scarifying the sensing spatial resolution, i.e., Z. Although the strain resolution of the DSS could be improved by padding zero, the cross correlation calculation time, i.e., demodulation time, was increased with the number of padding zeros increases. Moreover, the fluctuation of strain distribution induced by laser noise would not be improved by increasing the number of padding zeros, but lead to performance redundancy. This indicated that the optimization of the NZP would reduce the calculation time.

TABLE I
STRAIN RMS NOISE FOR SMF AND E-SMF UNDER SPATIAL RESOLUTIONS OF 1, 2, 5, 10, 20, 50, AND 100 MM, RESPECTIVELY

Spatial resolution	SMF	E-SMF
1.0 mm	34.80738	4.4761
2.0 mm	8.3326	1.87037
5.0 mm	3.07711	0.78386
10.0 mm	1.23737	0.61132
20.0 mm	0.7684	0.51862
50.0 mm	0.58956	0.4594
100.0 mm	0.4598	0.38397

III. EXPERIMENTAL RESULTS AND DISCUSSIONS

As shown in Fig. 2(b), an AZP method for calculating the number of padding zeros was proposed to optimize the NZP, where the principle was that the strain resolution should be lower than that of strain root mean square (rms) noise. The number of sampling points in a sliding window was set as 1, 2, 5, 10, 20, 50, and 100 mm, respectively, for SMF and E-SMF. Then, the strain distribution along the FUT was calculated by using the traditional cross correlation method under zero strain. Subsequently, the rms noises of the obtained strain distribution, i.e., σ, were calculated under the set sliding window, such as 1 mm. Then, resetting the sliding window as 2 mm and repeat afore-process to obtain the strain RMS noise. In this way, the strain RMS noise for SMF and E-SMF could be calculated under spatial resolutions of 1, 2, 5, 10, 20, 50, and 100 mm, respectively, as shown in Table I.

Obviously, the strain RMS noise of E-SMF is significantly smaller than that of SMF, due to enhanced RBS intensity of E-SMF, i.e., higher SNR. By performing quadratic exponential fitting on the afore-obtained scatter points, the fitting curve, i.e., $F(z, \sigma)$, between the strain RMS noise, i.e., σ, and spatial resolution, i.e., Z, for SMF and E-SMF could be expressed as follows:

$$\sigma = 11.89 * e^{(-1.139z)} + 0.6741 * e^{(-0.006635z)} \tag{6}$$

$$\sigma = 223.5 * e^{(-2.013z)} + 5.617 * e^{(-0.1287z)} \tag{7}$$

as shown in Fig. 3. Thus, the strain RMS noise at different spatial resolutions could be obtained according to (6) and (7). Assuming the strain rms noise under the spatial resolution of 1.5 mm is σ_1, then the NZP, i.e., P, could be calculated as follows:

$$P = \frac{\Delta F}{\sigma_1} - N.$$

Compared with the NZP of 2097152 for the traditional method (TM), the NZP is 8743 for AZP under the same spatial

Authorized licensed use limited to: SHENZHEN UNIVERSITY. Downloaded on October 29,2024 at 03:28:24 UTC from IEEE Xplore. Restrictions apply.

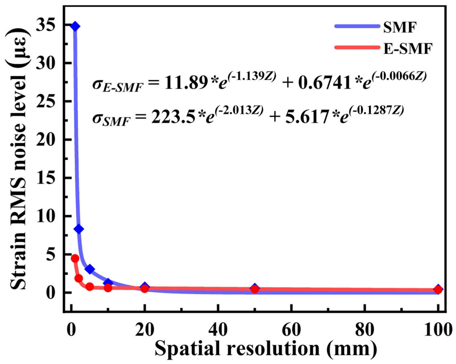

Fig. 3. Obtained fitting curve between the strain RMS noise, i.e., σ, and spatial resolution, i.e., Z, for SMF and E-SMF, labeled by violet and red, respectively.

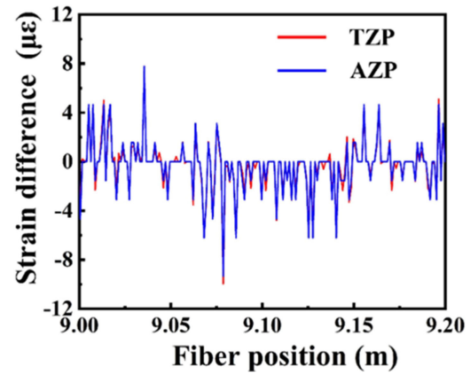

Fig. 4. Comparison of the noise levels, i.e., strain differences, between traditional and AZP methods based on E-SMF under the spatial resolution of 2.0 mm, when no strain was applied.

TABLE II
PERFORMANCE COMPARISON BETWEEN AZP AND TZP

SR \ Method	AZP		TZP	
	NZP	Time	NZP	Time
4.5 mm	34760	0.829s	2097152	45.651s
3.0 mm	23465	0.731s	2097152	83.683s
1.5 mm	8743	0.476s	2097152	138.842s

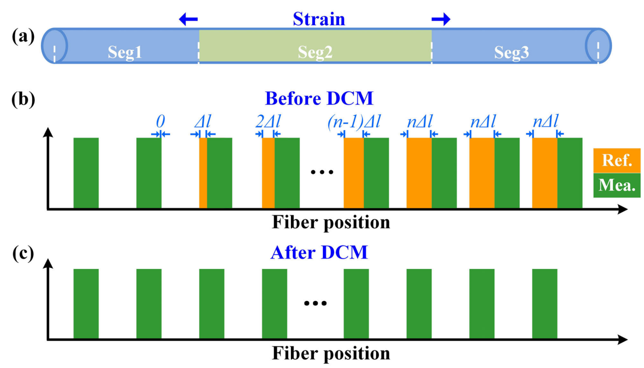

Fig. 5. (a) Schematic of the sensing segment of FUT, i.e., seg1, seg2, and seg3, where the strain was applied to seg2; position deviation between Ref. and Mea. spectrum (b) before and (c) after DCM, respectively. Note that the orange and green blocks present the data size of the Ref. and Mea. spectra for a single measuring point, respectively.

resolution, i.e., 1.5 mm, as shown in Table II. Moreover, the NZP and calculation time were increased to 34 760 and 0.829 s, respectively, under the spatial resolution of 4.5 mm. The larger the sliding window is, the more accurate the cross correlation, and the lower the strain rms noise. Thus, much NZP should be padded to make the spectral resolution better than strain rms noise. Compared with TZP, the cross correlation calculation time was improved from 138.842 to 0.476s by using the proposed AZP method under the spatial resolution of 1.5 mm, indicating that the cross correlation calculation time was reduced by nearly 300×.

To investigate the reduction of the NZP, the strain difference, i.e., noise level, caused by laser and environment in the OFDR system was compared under the spatial resolution of 1.5 mm. As shown in Fig. 4, in the zero-strain section, i.e., position between 9.00 and 9.20 m, the strain difference calculated using AZP and TZP overlapped well, corresponding to NZP of 8743 2 097 152. Obviously, the strain difference is within $\pm 8\ \mu\varepsilon$. This indicated that the reduction of the NZP for the AZP method has no effect on the strain sensing performance, but greatly improves the calculation time.

As shown in Fig. 5(a), the FUT was divided into three segments, i.e., seg1, seg2, and seg3, where the external strain was applied to seg2. Note that the orange and green blocks present the data size of the Ref. and Mea. spectra for a single measuring point, respectively. As shown in Fig. 5(b), the Ref. and Mea. spectrum in seg1, i.e., without strain, was completely consistent. But in seg2, i.e., with strain, the position deviation induced by the elastic-optic effect was accumulated along the fiber, where the maximum position deviation was $n\Delta l$ at the fiber end.

As shown in Fig. 6(a), the cross correlation peak between Ref. and Mea. spectrum in the seg2 could not be identified due to deteriorated similarity induced by large position deviation, i.e., $n\Delta l$, indicating that the cross correlation spectra would be deteriorated due to the position deviation. To obtain a cross correlation peak with a larger amplitude, a DCM was proposed, as illustrated in Fig. 2(a). Based on afore-obtained cross correlation spectrum shift, i.e., Δf, a transformation was conducted to acquire the position deviation, i.e., Δl, which could be given by the following equation:

$$\Delta l = kZ\Delta f \tag{8}$$

where k is the coefficient of strain sensitivity. Therefore, the next fiber section, i.e., L_{i+1}, was compensated by the calculated position deviation, i.e., Δl [15], [16], [20], [21]. Finally, the distributed strain along the FUT could be obtained by repeating the above process until the last fiber section. As shown in Fig. 6(b), the amplitude of the cross correlation peak was improved to 0.835 after the DCM, indicating that the deteriorated similarity was induced by position deviation between the Ref. and Mea. signal could be greatly improved by using DCM.

To verify the proposed DCM based on the AZP method, the strain property of the E-SMF and SMF was investigated,

Authorized licensed use limited to: SHENZHEN UNIVERSITY. Downloaded on October 29,2024 at 03:28:24 UTC from IEEE Xplore. Restrictions apply.

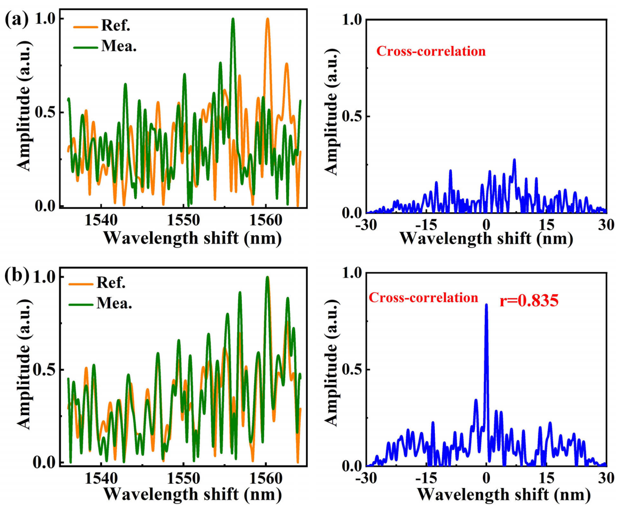

Fig. 6. Obtained similarity and cross correlation peak at the seg2 between Ref. and Mea. spectrum (a) before and (b) after using DCM. Note that the cross correlation peak in (a) could not be identified due to large position deviation, i.e., $n\Delta l$, in Fig. 5.

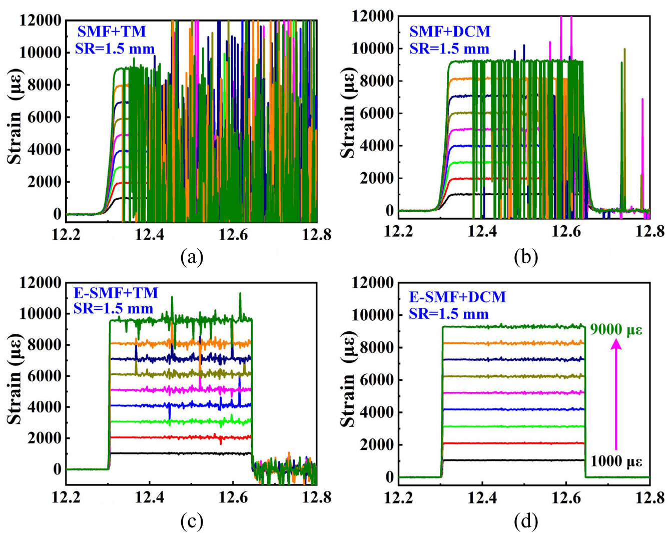

Fig. 7. Demodulated strain profiles based on (a) and (b) SMF, and (c) and (d) E-SMF using TM and DCM, respectively, when the applied strain was increased from 0 to 9000 $\mu\varepsilon$ with a step of 1000 $\mu\varepsilon$ under a spatial resolution of 1.5 mm.

respectively. Compared with SMF, the RS intensity of the E-SMF was enhanced by using UV exposure [13]. In the experiment, two methods without and with DCM based on AZP were compared, corresponding to TM and DCM, when the strain was increased from 1000 to 9000 $\mu\varepsilon$. As shown in Fig. 7(a), the demodulated strain in the rear strain-section and zero-strain-section was submerged in noise, when the applied strain is greater than 2000 $\mu\varepsilon$. The reason for this phenomenon is the accumulated position deviation caused by the applied strain. After using DCM, the rear zero-strain section, i.e., position between 12.65 and 12.8 m, for the SMF was effectively improved, as shown in Fig. 7(b). However, there were still many wrong points in the stretched-strain section using DCM based on SMF. This indicated that the wrong points induced by lower SNR could not be

TABLE III
SENSING PERFORMANCE COMPARISON BASED ON DIFFERENT METHODS

Work	Method	Sweeping range (nm)	Spatial Resolution (mm)	Max. Strain (με)
Ref. [18]	Distance compensation and image wavelet denoising	10	2.56	2000
Ref. [19]	Local similarity of RS spectrum	20	3	3000
Ref. [21]	Spectrum registration and spatial calibration	20	5	7000
Ref. [20]	Distance compensation	40	2	10000
Ref. [22]	Image denoising (wavelet transform and Gaussian filter)	40	4	7000
This work	E-SMF and distance compensation	30	1.5	9000

solved. Therefore, the exposed SMF with an enhanced RBS intensity was employed. As shown in Fig. 7(c), the strain profile demodulated by TM could be generally identified in the stretched-strain section, but with obvious fluctuation in the zero-strain section. Compared with SMF using TM or DCM, the strain profile could be demodulated correctly even if the TM was used, attributing to the high RS of the E-SMF. As shown in Fig. 7(d), the strain profile of the E-SMF could be successfully and well demodulated in the zero- and stretched-strain section at the spatial resolution of 1.5 mm by using DCM, indicating that a wide-strain range, i.e., up to 9000 $\mu\varepsilon$, could be achieved by combining E-SMF with DCM.

Finally, the sensing performance based on different methods is listed in Table III. Although the spatial resolution and maximum measured strain have been improved by using DC and image wavelet denoising alone, or a combination of both, or other methods [18], [19], [20], [21], [22], these additional algorithms have brought huge computational burden to the already complex OFDR data processing process. In this work, a DSS with a spatial resolution of 1.5 mm under the strain of 9000 $\mu\varepsilon$ was exhibited by using E-SMF combined with DC based on AZP, which reduced the computational complexity.

IV. CONCLUSION

In conclusion, a high-spatial-resolution, i.e., 1.5 mm, DSS based on E-SMF, was experimentally demonstrated, where the strain Mea. range was up to 9000 $\mu\varepsilon$. A tradeoff existed between the strain resolution and sensing spatial resolution. An AZP method was proposed to optimize the NZP to reduce the calculation time based on the principle that the strain resolution should be lower than that of strain RMS noise. Moreover, the cross correlation calculation time was reduced by nearly 300× under a spatial resolution of 1.5 mm. Furthermore, an efficient method of combing AZP with DCM without an extra algorithm based on E-SMF was proposed to realize wide-range strain sensing.

Authorized licensed use limited to: SHENZHEN UNIVERSITY. Downloaded on October 29,2024 at 03:28:24 UTC from IEEE Xplore. Restrictions apply.

References

[1] C. Monsberger and W. Lienhart, "Distributed fiber optic shape sensing of concrete structures," *Sensors*, vol. 21, no. 18, p. 6098, Sep. 2021.

[2] F. Peng, H. Wu, X. Jia, Y. Rao, Z. Wang, and Z. Peng, "Ultra-long high-sensitivity Φ-OTDR for high spatial resolution intrusion detection of pipelines," *Opt. Exp.*, vol. 22, no. 11, pp. 13804–13810, Jun. 2014.

[3] S. Sharma, V. Chaudhary, and D. Kumar, "Design of chemical sensor based on dual core photonic crystal fiber," *Mater. Today, Proc.*, vol. 33, no. 5, pp. 2122–2124, 2020.

[4] G. P. Mishra, D. Kumar, V. S. Chaudhary, and S. Kumar, "Design and sensitivity improvement of microstructured-core photonic crystal fiber based sensor for methane and hydrogen fluoride detection," *IEEE Sensors J.*, vol. 22, no. 2, pp. 1265–1272, Jan. 2022.

[5] V. S. Chaudhary, D. Kumar, and S. Kumar, "SPR-assisted photonic crystal fiber-based dual-wavelength single polarizing filter with improved performance," *IEEE Trans. Plasma Sci.*, vol. 49, no. 12, pp. 3803–3810, Dec. 2021.

[6] V. S. Chaudhary, D. Kumar, B. P. Pandey, and S. Kumar, "Advances in photonic crystal fiber-based sensor for detection of physical and biochemical parameters—A review," *IEEE Sensors J.*, vol. 23, no. 2, pp. 1012–1023, Jan. 2023.

[7] X. Liu et al., "Feasibility analysis of an SMS-/MSM-/SMSMS-based optical fiber sensor structure," *Appl. Opt.*, vol. 61, no. 9, pp. 2327–2332, Mar. 2022.

[8] S. Qu et al., "Distributed sparse signal sensing based on compressive sensing OFDR," *Opt. Lett.*, vol. 45, no. 12, pp. 3288–3291, Jun. 2020.

[9] H. Qian et al., "Distributed dynamic strain sensing in coherent Φ-OTDR with a pulse conversion algorithm," *Opt. Lett.*, vol. 46, no. 7, pp. 1668–1671, Apr. 2021.

[10] M. Froggatt and J. Moore, "High-spatial-resolution distributed strain measurement in optical fiber with Rayleigh scatter," *Appl. Opt.*, vol. 37, no. 10, p. 1735, Apr. 1998.

[11] R. Chen et al., "Spatially resolved fibre cavity ring down spectroscopy," *Sci. Rep.*, vol. 10, p. 20167, Nov. 2020.

[12] K. Feng et al., "Enhancement of the performance and data processing rate of an optical frequency domain reflectometer distributed sensing system using a limited swept wavelength range," *Sensors*, vol. 18, no. 10, p. 3480, Oct. 2018.

[13] S. Loranger, M. Gagne, V. Lambin-Iezzi, and R. Kashyap, "Rayleigh scatter based order of magnitude increase in distributed temperature and strain sensing by simple UV exposure of optical fibre," *Sci. Rep.*, vol. 5, p. 11177, Jun. 2015.

[14] C. Du et al., "High-spatial-resolution strain sensor based on Rayleigh-scattering-enhanced SMF using direct UV exposure," *J. Lightw. Technol.*, vol. 41, no. 5, pp. 1566–1570, Mar. 1, 2023.

[15] A. Yan et al., "Distributed optical fiber sensors with ultrafast laser enhanced Rayleigh backscattering profiles for real-time monitoring of solid oxide fuel cell operations," *Sci. Rep.*, vol. 7, p. 9360, Aug. 2017.

[16] Y. Meng et al., "Submillimeter-spatial-resolution φ-OFDR strain sensor using femtosecond laser induced permanent scatters," *Opt. Lett.*, vol. 47, no. 23, p. 6289, Dec. 2022.

[17] P. Lu, S. J. Mihailov, D. Coulas, H. Ding, and X. Bao, "Low-loss random fiber gratings made with an fs-IR laser for distributed fiber sensing," *J. Lightw. Technol.*, vol. 37, no. 18, pp. 4697–4702, Sep. 15, 2019.

[18] P. Li et al., "High-spatial-resolution strain sensor based on distance compensation and image wavelet denoising method in OFDR," *J. Lightw. Technol.*, vol. 39, no. 19, pp. 6334–6339, Jul. 9, 2021.

[19] K. Feng et al., "Improvement of the strain measurable range of an OFDR based on local similar characteristics of a Rayleigh scattering spectrum," *Opt. Lett.*, vol. 43, no. 14, p. 3293, Jul. 2018.

[20] S. Qu, Z. Wang, Z. Qin, Y. Xu, Z. Cong, and Z. Liu, "Internet of Things infrastructure based on fast, high spatial resolution, and wide measurement range distributed optic-fiber sensors," *IEEE Internet Things J.*, vol. 9, no. 4, pp. 2882–2889, Feb. 2022.

[21] S. Zhao, J. Cui, L. Suo, Z. Wu, D.-P. Zhou, and J. Tan, "Performance investigation of OFDR sensing system with a wide strain measurement range," *J. Lightw. Technol.*, vol. 37, no. 15, pp. 3721–3727, Aug. 1, 2019.

[22] S. Qu, Z. Qin, Y. Xu, Z. Cong, Z. Wang, and Z. Liu, "Improvement of strain measurement range via image processing methods in OFDR system," *J. Lightw. Technol.*, vol. 39, no. 19, pp. 6340–6347, Oct. 1, 2021.

[23] Z. Ding et al., "Compensation of laser frequency tuning nonlinearity of a long range OFDR using deskew filter," *Opt. Exp.*, vol. 21, no. 3, p. 3826, Feb. 2013.

Cailing Fu was born in Hubei, China, in 1989. She received the M.S. degree in optical engineering from the Wuhan Institute of Technology, Wuhan, China, in 2015, and the Ph.D. degree in optical engineering from Shenzhen University, Shenzhen, China, in 2018.

From 2018 to 2020, she was a Postdoctoral Research Fellow with Information and Communication Engineering, Shenzhen University, where she has been an Associate Professor, since June, 2020. She has authored or coauthored more than 50 journals and conference papers. Her current research interests focus on distributed optical fiber sensing technology.

Chao Du was born in Shanxi, China, in 1998. He received the B.S. degree from the Taiyuan University of Technology, Taiyuan, China, in 2020, and the M.S. degree in optical engineering from Shenzhen University, Shenzhen, China, in 2023.

His current research interests include distributed optical fiber sensing technology.

Rongyi Shan was born in Guangdong, China, in 1999. He received the B.S. degree from the Guangdong University of Technology, Guangzhou, China, in 2022.

His current research interests include distributed optical sensing.

Zhenwei Peng was born in Guangdong, China, in 1999. He received the B.S. degree from the Changchun University of Science and Technology, Changchun, China, in 2021.

His current research interests include fiber Bragg grating array.

Ronglong Sui was born in Ganzhou, China, in 1998. He received the B.S. degree from Nanchang Hangkong University, Nanchang, China, in 2021. He is currently pursuing the master's degree in optical engineering with Shenzhen University, Shenzhen, China.

His main research interests include distributed fiber optic sensing and femtosecond laser processing.

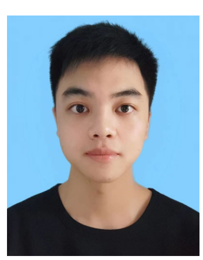

Huajian Zhong was born in Jiangxi, China, in 1998. He received the B.S. degree from the Changchun University of Science and Technology, Changchun, China, in 2020. He is currently pursuing the Ph.D. degree in optical engineering with Shenzhen University, Shenzhen, China.

His current research interests include distributed optical sensing.

Authorized licensed use limited to: SHENZHEN UNIVERSITY. Downloaded on October 29,2024 at 03:28:24 UTC from IEEE Xplore. Restrictions apply.

Yanjie Meng was born in Guangling, China, in 1994. He received the M.S. degree from the China University of Mining and Technology, Xuzhou, China, in 2019 and the Ph.D. degree in optical engineering from Shenzhen University, Shenzhen, China, in 2023.

His main research interests include optical fiber shape sensing and femtosecond laser processing.

Wenfa Liang was born in Guangdong, China, in 1999. He received the bachelors degree from the Dongguan University of Technology, Dongguan, China, in 2018.

His research interests include signal demodulation based on FPGA and fiber optic shape sensing.

Shuai Xiao was born in Hengyang, China, in 2001. He received the B.E. degree from Jiangsu Normal University, Xuzhou, China, in 2022.

His main research interests include optical fiber shape sensing.

Yuhao Kong was born in Qufu, China, in 1999. He received the bachelor's degree from the Hefei University of Technology, Hefei, China, in 2022.

His main research interests include femtosecond laser processing.

Xiaoyu Yin was born in Chongqing, China, in 1974.

Since 2012, she has been with Shenzhen University, Shenzhen, China.

Yiping Wang (Senior Member, IEEE) was born in Chongqing, China, in 1971. He received the B.Eng. degree in precision instrument engineering from the Xi'an Institute of Technology, Xi'an, China, in 1995, the M.S. and Ph.D. degrees in optical engineering from Chongqing University, Chongqing, in 2000 and 2003, respectively.

From 2003 to 2005, he was a Postdoctoral Fellow with Shanghai Jiao Tong University, Shanghai, China. From 2005 to 2007, he was a Postdoctoral Fellow with the Hong Kong Polytechnic University, Hong Kong. From 2007 to 2009, he was a Humboldt Research Fellow with the Institute of Photonic Technology (IPHT), Jena, Germany. From 2009 to 2011, he was with the Optoelectronics Research Center (ORC), University of Southampton, Southampton, U.K., as a Marie Curie Fellow. Since 2012, he has been with Shenzhen University, Shenzhen, China, as a Distinguished Professor. He has authored or coauthored one book, 21 patent applications, and more than 240 journals and conference papers. His current research interests include optical fiber sensors, fiber gratings, and photonic crystal fibers.

Prof. Wang is a Senior Member of the Optical Society of America, and the Chinese Optical Society.

Authorized licensed use limited to: SHENZHEN UNIVERSITY. Downloaded on October 29,2024 at 03:28:24 UTC from IEEE Xplore. Restrictions apply.